NASA TECHNICAL MEMORANDUM

NASA TM X-2170

NASA TM X-2170

STATIC-PRESSURE CONTOURS IN THE BLADE PASSAGE AT THE TIP OF SEVERAL HIGH MACH NUMBER ROTORS

by Genevieve R. Miller and Everett E. Bailey

Lewis Research Center

Cleveland, Ohio 44135

NATIONAL AERONAUTICS AND SPACE ADMINISTRATION • WASHINGTON, D. C. • FEBRUARY 1971

1. Report No.	2. Government Accession No.	3. Recipient's Catalog No.
NASA TM X-2170		

4. Title and Subtitle	5. Report Date
STATIC-PRESSURE CONTOURS IN THE BLADE PASSAGE AT THE TIP OF SEVERAL HIGH MACH NUMBER ROTORS	February 1971
	6. Performing Organization Code
7. Author(s)	8. Performing Organization Report No.
Genevieve R. Miller and Everett E. Bailey	E-5875
	10. Work Unit No.
9. Performing Organization Name and Address	720-03
Lewis Research Center National Aeronautics and Space Administration Cleveland, Ohio 44135	11. Contract or Grant No.
	13. Type of Report and Period Covered
12. Sponsoring Agency Name and Address	Technical Memorandum
National Aeronautics and Space Administration Washington, D. C. 20546	14. Sponsoring Agency Code

15. Supplementary Notes

16. Abstract

Static pressure contours across the blade passage at the tip of three high Mach number rotors are presented. Inlet relative Mach numbers vary from 1.23 to 1.59. Flow rates vary from near choke values to those near blade stall. Blade shapes include both double circular arc and multiple circular arc. The static pressure contour plots indicate the location of the passage shock waves over a range of Mach numbers and operating conditions. Qualitative comparisons of flow conditions through blade passages for the two blade shapes can be made. However, a quantitative analysis of the data is not attempted.

17. Key Words (Suggested by Author(s))	18. Distribution Statement
Compressor High Mach number Rotors Static pressure contours	Unclassified - unlimited

19. Security Classif. (of this report)	20. Security Classif. (of this page)	21. No. of Pages	22. Price*
Unclassified	Unclassified	17	$3.00

*For sale by the National Technical Information Service, Springfield, Virginia 22151

STATIC-PRESSURE CONTOURS IN THE BLADE PASSAGE AT THE TIP OF SEVERAL HIGH MACH NUMBER ROTORS

by Genevieve R. Miller and Everett E. Bailey

Lewis Research Center

SUMMARY

Static pressure contours across the blade passage at the tip of three high Mach number rotors were made for inlet relative Mach numbers varying from 1.23 to 1.59. Flow rates for these contours vary from values near choke to those near blade stall. Blade shapes are both double circular arc and multiple circular arc.

The static pressure contour plots indicate the location of the passage shock waves over a range of Mach numbers and operating conditions. Also, they allow qualitative comparisons of flow conditions through blade passages for the two blade shapes. However, because of the indeterminable effects of three-dimensional flow, data reduction techniques, and probe size on the accuracy of the static pressures, a quantitative analysis of the data is not attempted.

INTRODUCTION

Blade speed and blade loading of axial-flow compressor stages are continually being increased in order to obtain a higher pressure ratio from individual stages. As the local velocities exceed the local sonic velocity, shock patterns occur throughout the blade passage. Associated with the shock formations are pressure losses in flow across the shock as well as increases in viscous losses and other effects due to interactions with the blade-surface boundary layers. The magnitude of both these effects increases with local flow Mach number and must be considered in an accurate appraisal or prediction of flow conditions across a blade row.

The investigations reported in references 1 and 2 used both analytical and experimental approaches to identify the shock patterns that occur in high-speed rotating compressor blade rows. From these studies flow models for predicting loss due to shock patterns in the blade passages were suggested.

Recently, the General Electric Company, under contract NAS3-7617 with NASA, experimentally evaluated the performance of a number of high Mach number compressor rotors. The results of this investigation are reported in references 3 to 6. Supplemental instrumentation used during this investigation included high-frequency static-pressure transducers mounted in the outer casing above the rotor blade tip. From these measurements the static-pressure field in the blade tip flow passages were constructed.

In this report the static pressure contours in the blade passage at the tip of three rotor blade rows are presented for speeds between 90 and 110 percent of design and for a range of flow rates. The test blade rows consisted of both double circular arc and multiple circular arc blade shapes and were tested over a Mach number range of 1.23 to 1.59. A detailed analysis of the results is not attempted in this report.

DESCRIPTION OF TEST ROTORS

Detailed aerodynamic and mechanical design features of the three rotors used in this investigation are presented in reference 3. In this report, only significant blade design variations will be given. The three rotors represent two blade shapes and two levels of blade loading (indicated herein by D-factor). The blade loading parameter D-factor is developed in reference 7. A value of tip D-factor of 0.35 is considered to be a medium level of loading. The rotor designated as II-D had blade sections in the tip region that were the familiar double circular arc form and had a tip D-factor of 0.45. The blade sections in the tip region of the other two rotors used a multiple circular arc blade shape. This type of blade section permits one rate of turning along the forward portion of the blade and another along the rear portion and thus permits some control of blade surface Mach number. Rotor II-B had the same D-factor as rotor II-D (D = 0.45), but with less turning in the forward part of the blade. The rotor I-B had an inlet portion the same as II-B but the design D-factor was lower. Table I summarizes the principal blade design variations and blade speeds at which data are presented.

ACQUISITION AND REDUCTION OF DATA

Local pressures over the rotating blade tip were obtained by combining (1) measurements of average static pressures from outer wall static-pressure taps with (2) measurements of the change in static pressure as obtained from high-response pressure transducers. These measurements were obtained from 10 static-pressure taps (covering the axial extent of the blade tip section) and 10 high-frequency pressure transducers (covering the same axial extent as the wall taps), which were mounted in the outer wall casing (see fig. 1). The transducers were of the quartz crystal type with a pressure sensitive

surface of approximately 0.22 inch (0.56 cm) diameter. The transducer-recording system had a frequency response of over 100 000 hertz. The changes in static pressure, as sensed by the crystal transducers, were displayed on an oscilloscope. Using an electronic triggering system, activated by a particular blade, a trace covering the static-pressure variation across two blade passages is displayed. The triggering device also insures that the same two blade passages are sampled each time. From the known blade tip section geometry and blade speed, the pressure trace and blade position can be related.

A trace of a typical pressure change across two adjacent blade passages is shown in figure 2. The blips over the trace are signals from the triggering device and were used to locate the trace with respect to the blades. On the trace, sharp pressure changes measured across the blade tip section (pressure to suction surfaces) and across a passage shock allow an approximate positioning of the shock in the flow passage.

Local values of static pressure on a given trace were obtained by determining an average value for each trace and relating it to the static pressure measured by the outer wall taps. The local pressure values were positioned in the blade passage by plotting the trace of absolute pressure with passage width as shown in figure 3. When this process was completed for the 10 crystal transducers used, points of equal pressure were connected to form pressure isobars. An example of the pressure isobar plots is shown in figure 4.

A number of factors make it difficult to estimate an accuracy value that could be applied generally to the static pressures presented. The sample trace shown in figure 2 illustrates several of these factors. First, the width of the band shown in figure 2, indicates the variations of pressure with time. Second, the trace also indicates that the pressure variations differ in the two adjacent blade passages. The data reduction procedure averages these time and space variations. Average values vary from the extreme values by as much as $\pm 1\frac{1}{2}$ psi (1.03 N/cm^2). Another indeterminable effect on the accuracy of the local pressure is the diameter of the pressure sensitive face of the probe. The pressure transducer used in this investigation had a diameter of 0.22 inch (0.56 cm), or nearly 10 percent of the passage width. It is assumed that the readout value is some average of the pressures over the entire area of probe face. In particular, this may result in smoothing out pressure peaks. Additional problem areas include the accurate alinement of the blades with the pressure traces and the effect of outer casing boundary-layer flows on measured pressures.

INTERPRETATION OF DATA

The pressure isobar plots (such as shown in fig. 4) are presented as essentially

two-dimensional maps. It should be recognized that there are three-dimensional flows present that have some indeterminable effect on the static pressure patterns measured. Sources of these three-dimensional flows include curvature in the casing wall, boundary-layers on the casing and blade surfaces, and blade tip clearance flows.

The position of shock waves in the blade passages is evidenced by sharp increases in static pressure and indicated by closely spaced pressure isobars. In particular, a bow wave lying just upstream of the blade leading edge and a passage shock can usually be identified.

A measure of the strength of the shock wave is indicated by the static pressure rise across the shock. Shock strength is related to the local Mach number of the flow and the angle between the flow direction and shock wave.

ROTOR PERFORMANCE

Design blade tip speed for all rotors was 1400 feet per second (426.7 m/sec), and inlet relative Mach numbers at the blade tip was near 1.4. The overall performance of the three rotors is presented in figure 5. Mass-averaged values of pressure ratio and efficiency are plotted as functions of corrected weight flow. The reading number printed beside each data point affords a quick reference to the high-frequency data to be presented and to blade element performance data in references 4 to 6. The effects of blade loading, blade speed, and blade shape on overall performance are all evident in the figures and are discussed in detail in references 4 to 6.

PRESENTATION OF STATIC PRESSURE PLOTS

Nineteen maps of the static pressure fields over the tips of rotating blade rows are presented in figures 6 to 10. Each figure displays pressure contours for a given speed and over a range of flows or back pressure. Parts (a) of these figures represent the flow conditions at the flow rate nearest to stall, and parts (d) (part (c) of fig. 10) show flow conditions at the lowest back pressure measured (near choke). The numbers on each contour is the static pressure in psia. Thus, figure 6 shows pressure maps of four flow conditions in the 2D rotor at 100 percent speed, figures 7 and 8 are for the 2B and 1B rotors, respectively, at 100 percent speed, and figures 9 and 10 are for the 1B rotor at speeds of 110 and 90 percent of design.

Table II lists pertinent information for the various pressure maps. This includes the inlet relative Mach number of the flow entering the blades, the suction surface incidence angle, the inlet static and relative total pressures, the outlet relative Mach num-

ber, and the outlet static pressure. These were obtained by extrapolating the data in the references to the tip radius or by extrapolating the data from static pressure taps in the outer casing. Also included are the reading numbers corresponding to those on the performance curves of figure 5.

A comparison of the minimum static pressures for rotor 2B (multiple circular arc blades) and rotor 2D (double circular arc blades) provides an opportunity to qualitatively evaluate the effect of blade shape on blade suction surface Mach number. One purpose of the reduced camber in the blade leading edge region, as designed into the multiple circular arc blade shape, was to reduce the Mach number of the flow on the suction surface upstream of the shock location. Both blade sections operated at approximately the same level of inlet Mach number and had the same overall design blade loading. The generally lower levels of minimum static pressure measured for rotor 2D (fig. 6) as compared with those for rotor 2B (fig. 7) indicate that higher suction surface Mach numbers did occur with the double circular arc blade shape. In this design the multiple circular arc blade shape did reduce the suction surface Mach number upstream of the shock. Comparative relative Mach number can be computed from the minimum static pressures and the blade suction inlet relative total pressures.

SUMMARY REMARKS

The static pressure fields in the blade tip region of these high-speed rotor blade rows operating over a range of Mach numbers and flow rates are presented in the form of static pressure contour plots. Inlet relative Mach numbers varied from 1.23 to 1.59. Flow rate varied from the choke value to that near blade stall. Results from both multiple circular arc and double circular arc blade shapes are presented.

Because of the indeterminable effects of three-dimensional flows, annulus boundary layers, data reduction techniques, and probe size on the accuracy of the reduced static pressures, a quantitative evaluation of this single set of data is not attempted. However, the results do provide additional insight into the transonic flow conditions across high-speed rotor blade rows and some qualitative and comparative conclusions can be reached. The reaction of the passage shock to the blade row back pressure, the significant interaction of shock with blade surface boundary layer, and the ability of the multiple circular arc blade to minimize the shock inlet Mach number are indicated.

Lewis Research Center,
National Aeronautics and Space Administration,
Cleveland, Ohio, October 5, 1970,
720-03.

REFERENCES

1. Schwenk, Francis C.; Lewis, George W.; and Hartmann, Melvin J.: A Preliminary Analysis of the Magnitude of Shock Losses in Transonic Compressors. NACA RM E57A30, 1957.

2. Miller, Genevieve R.; Lewis, George W., Jr.; and Hartmann, Melvin J.: Shock Losses in Transonic Compressor Blade Rows. Paper 60-WA-77, ASME, Nov. 1960.

3. Seyler, D. R.; and Smith, Leroy H., Jr.: Single Stage Experimental Evaluation of High Mach Number Compressor Rotor Blading. Part 1: Design of Rotor Blading. Rep. R66FPD321, pt. 1, General Electric Co. (NASA CR-54581), Apr. 1, 1967.

4. Seyler, D. R.; and Gostelow, J. P.: Single Stage Experimental Evaluation of High Mach Number Compressor Rotor Blading. Part 2: Performance of Rotor 1B. Rep. R67FPD236, General Electric Co. (NASA CR-54582), Sept. 22, 1967.

5. Krabacher, K. W.; and Gostelow, J. P.: Single Stage Experimental Evaluation of High Mach Number Compressor Rotor Blading. Part 4: Performance of Rotor 2D. Rep. R67FPD276, General Electric Co. (NASA CR-54584), Oct. 6, 1967.

6. Gostelow, J. P.; and Krabacher, K. W.: Single Stage Experimental Evaluation of High Mach Number Compressor Rotor Blading. Part 5: Performance of Rotor 2B. Rep. R67FPD278, General Electric Co. (NASA CR-54585), Oct. 13, 1967.

7. Lieblein, Seymour; Schwenk, Francis C.; and Broderick, Robert L.: Diffusion Factor for Estimating Losses and Limiting Blade Loadings in Axial-Flow-Compressor Blade Elements. NACA RM E53D01, 1953.

TABLE I. - PRINCIPAL BLADE DESIGN VARIATIONS

Rotor designation	Blade speed, percent of design	Design blade loading tip	Blade shapes
I-B	110 100 90	0.35	MCA
II-B	100	0.45	MCA
II-D	100	0.45	DCA

TABLE II. - FLOW CONDITIONS FOR PRESSURE CONTOUR MAPS

Rotor	Percent of design speed	Reading number	Figure	Inlet relative Mach number, $M'_{1,e}$	Suction surface incidence angle, i_{ss}, deg	Inlet static pressure, p_{1e}		Relative total pressure, P'_{1e}		Outlet relative Mach number, M'_2	Outlet static pressure, p_2	
						psi	N/cm^2	psi	N/cm^2		psi	N/cm^2
2D	100	9	6a	1.454	0.1	12.51	8.62	42.98	29.61	0.736	20.24	13.95
		17	6b	1.455	-.3	12.24	8.43	42.11	29.01	.787	19.97	13.76
		14	6c	1.459	-.8	11.51	7.93	39.83	27.44	.951	18.15	12.51
		11	6d	1.468	-.9	10.92	7.52	38.28	26.37	1.302	13.20	9.09
2B	100	53	7a	1.435	1.3	12.63	8.70	42.23	29.10	0.756	21.03	14.49
		19	7b	1.453	.6	12.31	8.48	42.23	29.10	.802	20.30	13.99
		18	7c	1.458	.4	12.07	8.32	41.71	28.74	.865	19.42	13.38
		14	7d	1.458	.4	11.30	7.79	39.05	26.91	1.248	13.33	9.18
1B	100	64	8a	1.384	3.8	13.12	9.04	40.82	28.12	0.756	21.11	14.54
		56	8b	1.413	1.8	12.64	8.71	40.97	28.23	.887	20.10	13.85
		55	8c	1.424	1.1	12.14	8.36	39.96	27.53	1.012	18.19	12.53
		65	8d	1.426	.9	11.79	8.12	38.92	26.82	1.233	13.95	9.61
1B	110	102	9a	1.558	2.4	13.12	9.04	52.42	36.12	0.792	22.54	15.53
		101	9b	1.565	1.8	12.80	8.82	51.72	35.64	.840	21.76	14.99
		95	9c	1.580	1.2	11.89	8.19	49.07	33.81	.950	20.35	14.02
		96	9d	1.587	.8	11.28	7.77	47.02	32.40	1.348	13.89	9.57
1B	90	73	10a	1.232	3.9	13.58	9.36	34.33	23.65	0.704	19.43	13.39
		67	10b	1.270	1.4	12.96	8.93	34.48	23.76	.879	17.87	12.31
		69	10c	1.280	.5	12.49	8.61	33.68	23.21	1.114	14.00	9.65

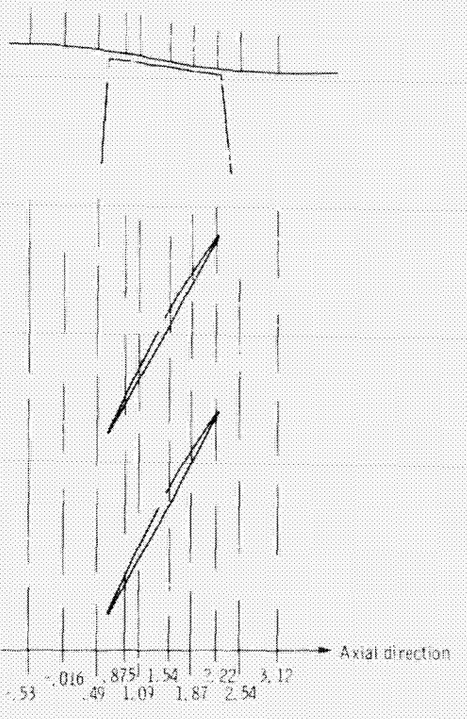

Figure 1. - Axial location of high-frequency pressure transducers.

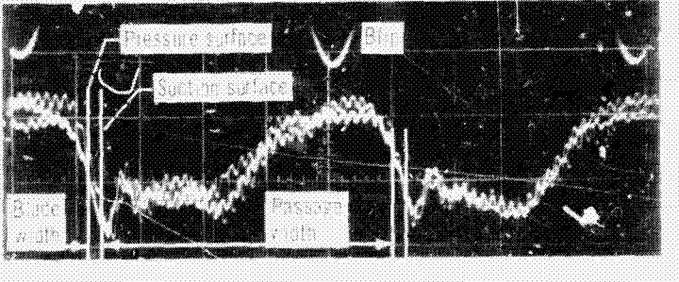

Figure 2. - Sample trace of pressure variation across two adjacent blades.

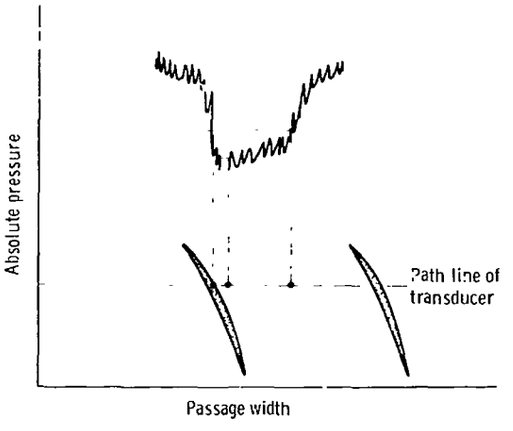

Figure 3. - Positioning of absolute pressures in blade passage.

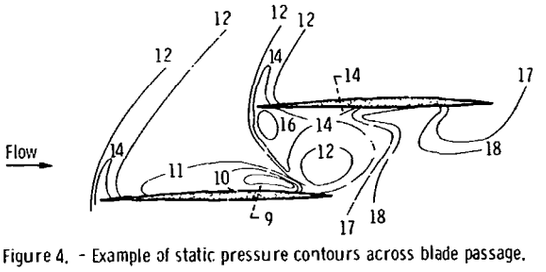

Figure 4. - Example of static pressure contours across blade passage.

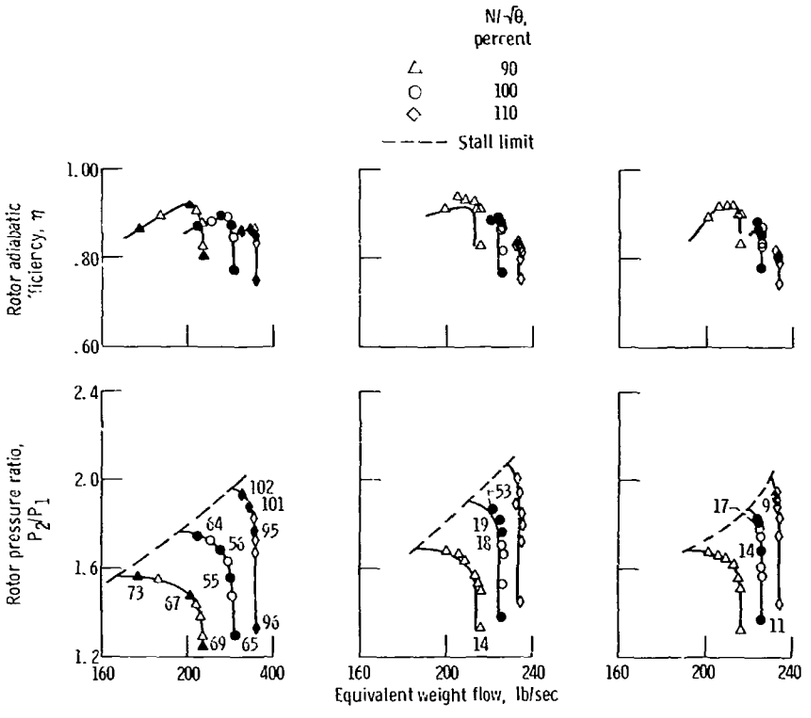

(a) Rotor 1B. (b) Rotor 2B. (c) Rotor 2D.

Figure 5. - Overall performance of test rotors (from refs. 4, 5, and 6).

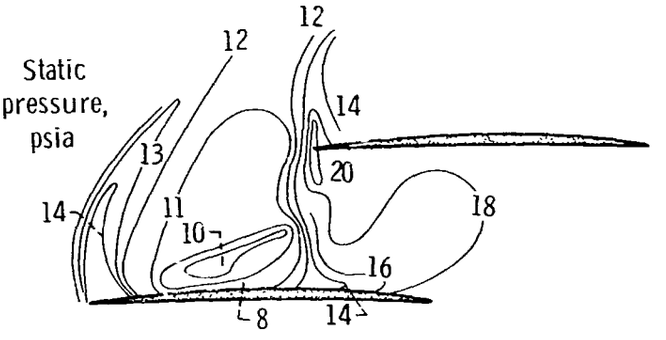

(a) Reading 9; near stall.

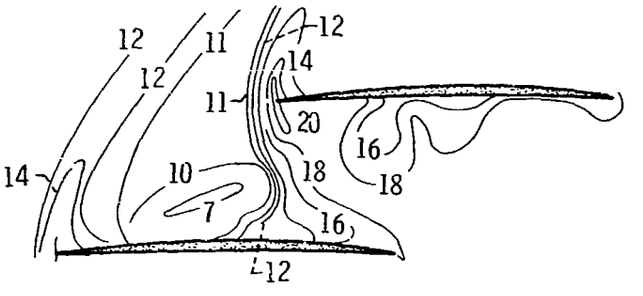

(b) Reading 17.

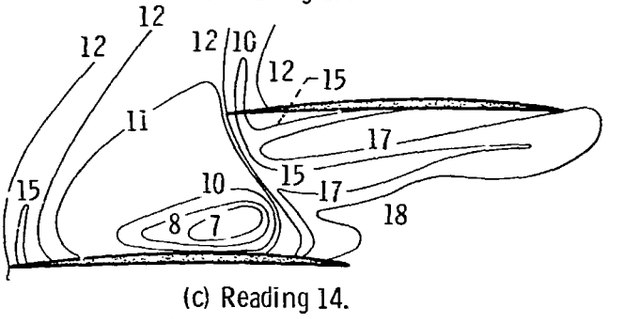

(c) Reading 14.

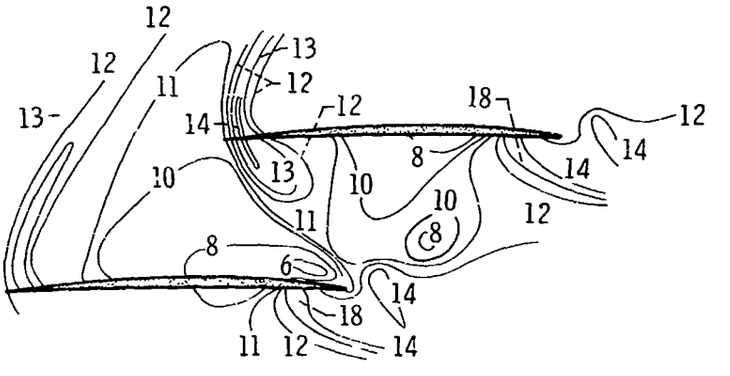

(d) Reading 11; near choke.

Figure 6. - Pressure contours for rotor 2D at 100 percent of design speed.

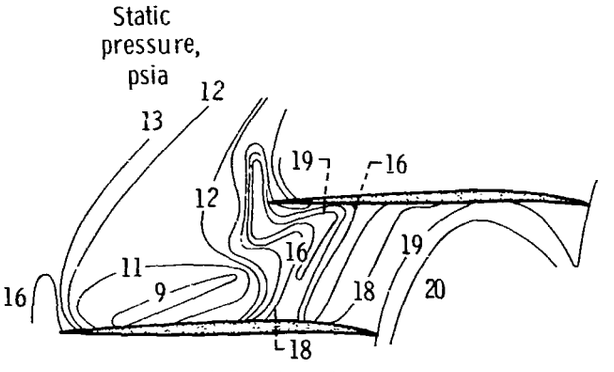

(a) Reading 53; near stall.

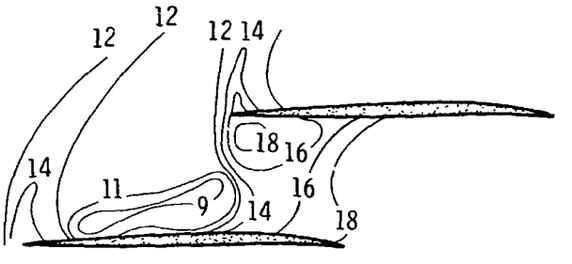

(b) Reading 19.

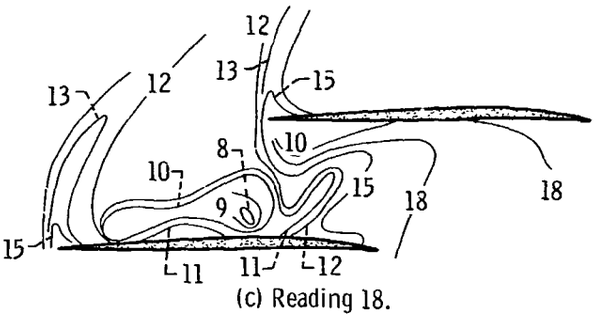

(c) Reading 18.

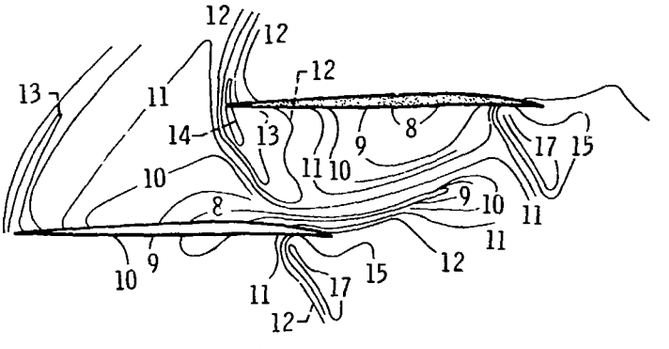

(d) Reading 14; near choke.

Figure 7. - Pressure contours for rotor 2B at 100 percent of design speed.

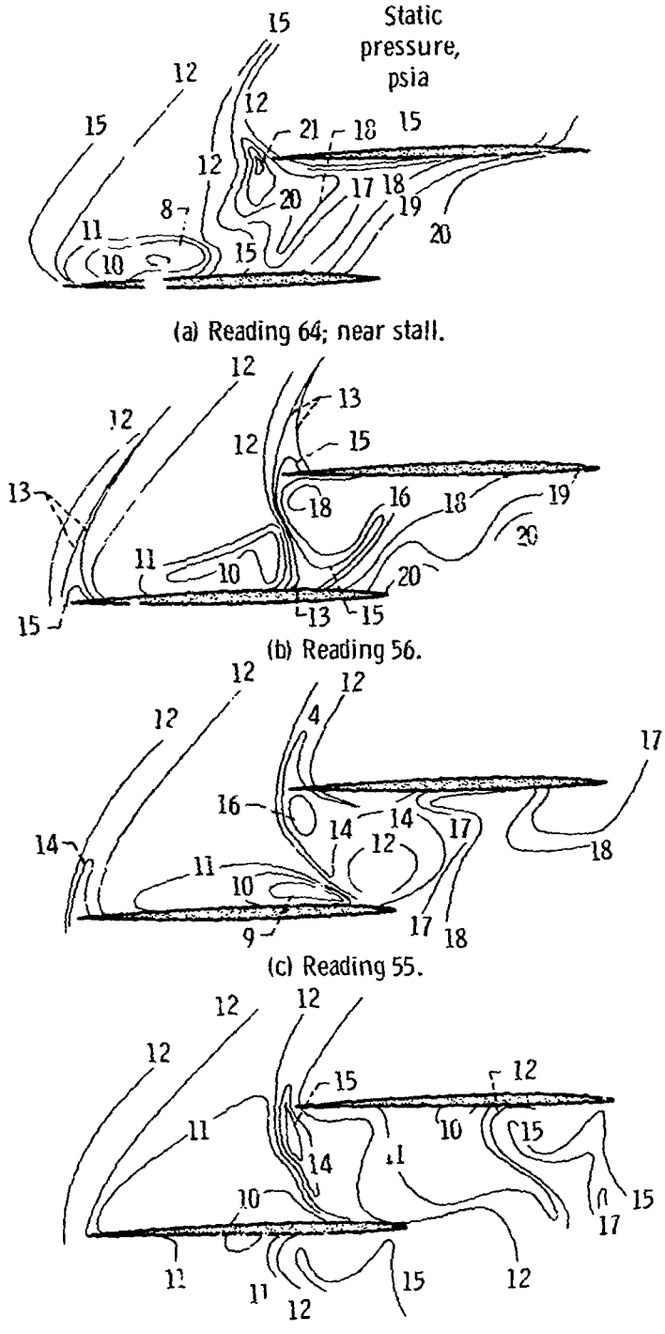

(a) Reading 64; near stall.

(b) Reading 56.

(c) Reading 55.

(d) Reading 65; near choke.

Figure 8. - Pressure contours for rotor 1B of 100 percent of design speed.

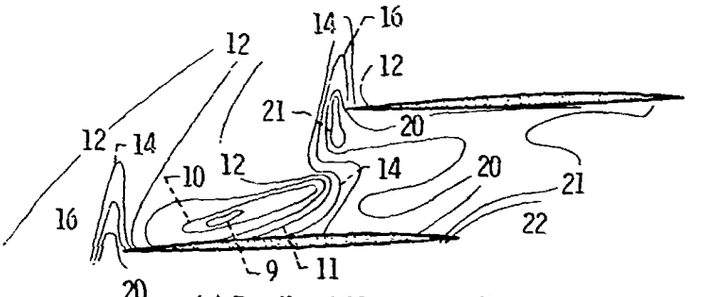

(a) Reading 102; near stall.

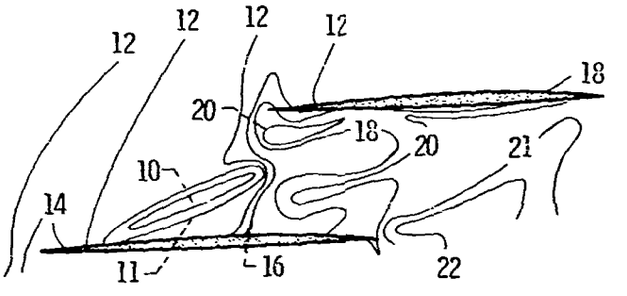

(b) Reading 101.

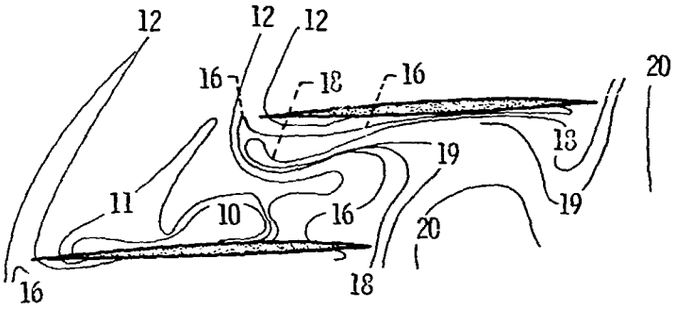

(c) Reading 95.

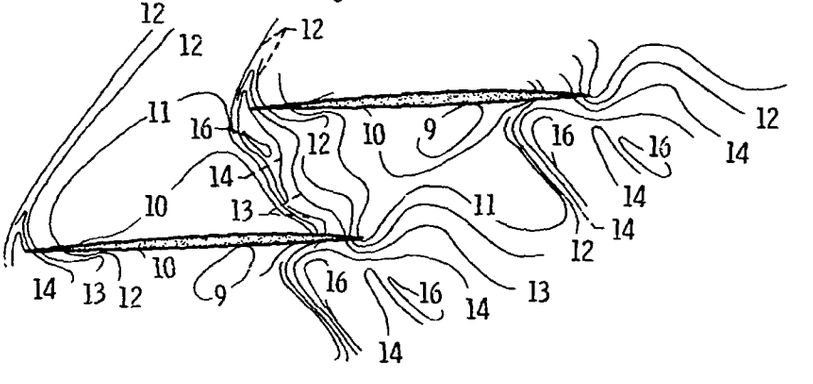

(d) Reading 96; near choke.

Figure 9. - Pressure contours of rotor 1B at 110 percent of design speed.

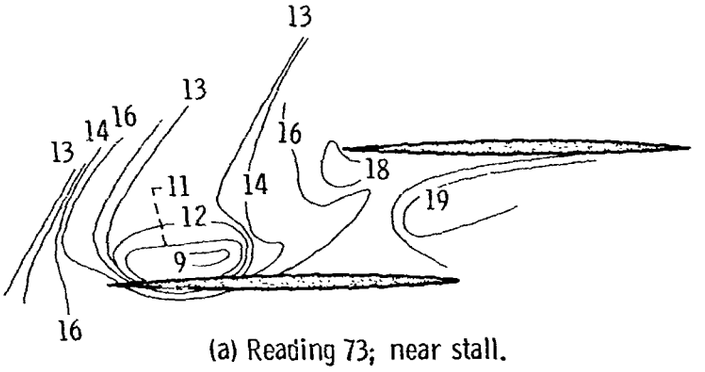

(a) Reading 73; near stall.

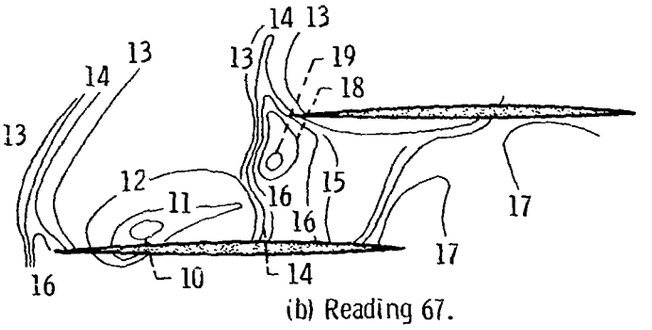

(b) Reading 67.

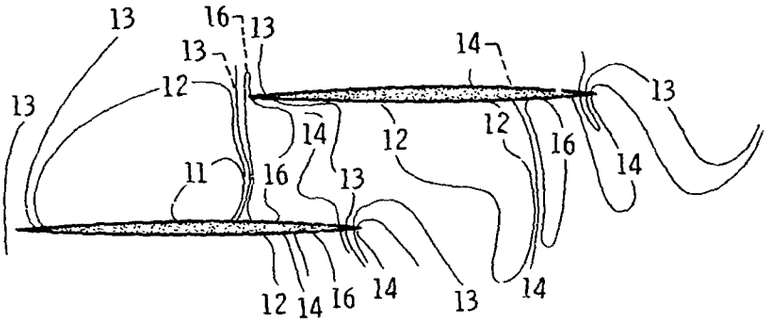

(c) Reading 69; near choke.

Figure 10. - pressure contour for rotor 1B at 90 percent of design speed.